Semiconductor superlattices in optoelectronic devices
Part 1: Superlattice structures and MBE growth

M. A. HERMAN

Institute of Vacuum Technology,
ul. Długa 44/50, 00-241 Warszawa, Poland
and Institute of Physics, Polish Academy of Sciences,
Al. Lotników 32/46, 02-668 Warszawa, Poland

1. Introduction

Modern electronics is built on the base of a well-established semiconductor technology. This technology has resulted in silicon integrated circuits, in optoelectronic devices made of III-V and II-VI semiconductor compounds, and in low-dimensional electron gas devices. It has also made feasible the manufacturing of semiconductor superlattice (SL) structures.

The term "semiconductor superlattice" is usually used to refer to a periodic structure of thin layers of two semiconductors positioned along one dimension. The period in thickness lies typically within the range from several to tens of nanometers. This is shorter than the mean free path of the electron in semiconductors, but longer than the crystal lattice constant. This periodic or superlattice potential modifies significantly the band structure of the host semiconductors, creating mini-zones in wave-vector space and subbands in energy. In such approach the superlattice can be considered as a new synthetized semiconductor, which is not present in the nature and exhibits unusual electronic and optical properties [1].

Essentially two types of superlattices may be distinguished. These are: compositional or heterojunction superlattices consisting of a periodic sequence of two semiconductors with different chemical composition, and doping superlattices consisting of a sequence of *n*-and *p*-doped layers with possibly undoped ones placed between them (so called *n-i-p-i*—crystals). The doping superlattices are grown in homogeneous semiconductor bulk.

The superlattice potential is induced in compositional superlattices by the periodic variation of the energy gap in the direction of crystal growth, whereas in *n-i-p-i*—crystals it is due to the electrostatic potential of fixed ionized impurities, which can be partly compensated by mobile electrons and holes confined in the *n*- and *p*-layers, respectively.

A number of new peculiarities related to electrostatic origin of the superlattice potential in *n-i-p-i*—crystals can be expected, in addition to the phenomena characteristic for compositional superlattices. The lowest electron and the uppermost hole subband states are locally separated each from the other (an indirect semiconductor in the real space). The electron-hole recombination can be naerly completely suppressed, depending on the design of the crystal. As a consequence, in these superlattices the effective energy gap as well as the electron and hole concentration can be varied arbitrarily over a wide range, either optically or by carrier injection into the bulk. In the paper the fundamentals of semiconductor superlattices, and the applications of these man-made structures in optoelectronic devices are presented.

2. Structures of semiconductor superlattices

Interest in semiconductor superlattices originates in 1970 with the proposal of Esaki and Tsu [2] to produce an one-dimensional periodic potential by means of a periodic variation of either impurities or alloy composition, with the period shorter than the electron mean free path. These authors have emphasized the compositional superlattice and have shown that unusual transport phenomena should occur in such "man-made" periodic structures.

Two years later Döhler [3] analyzed in great details the electronic properties of doping superlattices, and predicted a number of new peculiarities which are specific for these *n-i-p-i*—crystals.

Since that time, the searching for novel periodic structures has found considerable attention in many laboratories. This has resulted in the present-day variety of semiconductor superlattices [1].

2.1. Compositional superlattices

The location of the energy band-edges of different semiconductors in the electronic energy space are most often compared using the vacuum level as a reference [1]. Such comparison can be done by introducing the electron affinity χ as a characteristic parameter related to the each considered semiconductor.

Electron affinity specifies the energy required to release an electron from the bottom of the conduction band of the semiconductor to the vacuum level. Thus, if a semiconductor is characterized by a larger value of χ, then its conduction band-edge is located lower in the electronic energy space, in opposition to a semiconductor with smaller value of χ. Using the vacuum level as a reference one can divide the compositional superlattices into three different types (Fig. 1).

In the type I superlattice (Fig. 1a) the conduction and valence band-edge discontinuities ΔE_c and ΔE_v have opposite signs, and the energy gaps $E_{g,i}$ overlap completely.

In the type II superlattice (Fig. 1b) the band-edge modulation has the same sign for conduction and valence bands, and the energy gaps are separated or overlap only partly.

Finally, the polytype superlattice (Fig. 1c) is a triple-constituent system in which a semiconductor with wide energy gap, acting as a potential barrier for electrons and holes, has been introduced.

The first compositional superlattice has been grown of $GaAs-Al_xGa_{1-x}As$ compound (type I superlattice). The sequence of layers and the profile of the real-space energy band of this superlattice are given in Fig. 2. The line-up of the bands in the heterointerfaces determines the potential barriers for electrons and holes, and thus defines the periodic superlattice potential in the conduction and valence bands. The characteristic feature of this superlattice is that the narrow-gap semiconductor sandwiched between two wide-gap semiconductors forms two square quantum wells (one for electrons and one for holes). The depths of these potential wells depend on how the energy gap difference $\Delta E_g = E_g(\text{AlGaAs}) - E_g(\text{GaAs})$ is divided into the band-edge discontinuities ΔE_c and ΔE_v.

According to many experimental results [4], the most trustworthy values of the $GaAs-Al_xGa_{1-x}As$ heterojunction band offsets are equal to $\Delta E_c = 0.60\ \Delta E_g$ and $\Delta E_v = 0.40\ \Delta E_g$ and are independent of Al mole fraction in the ternary compound.

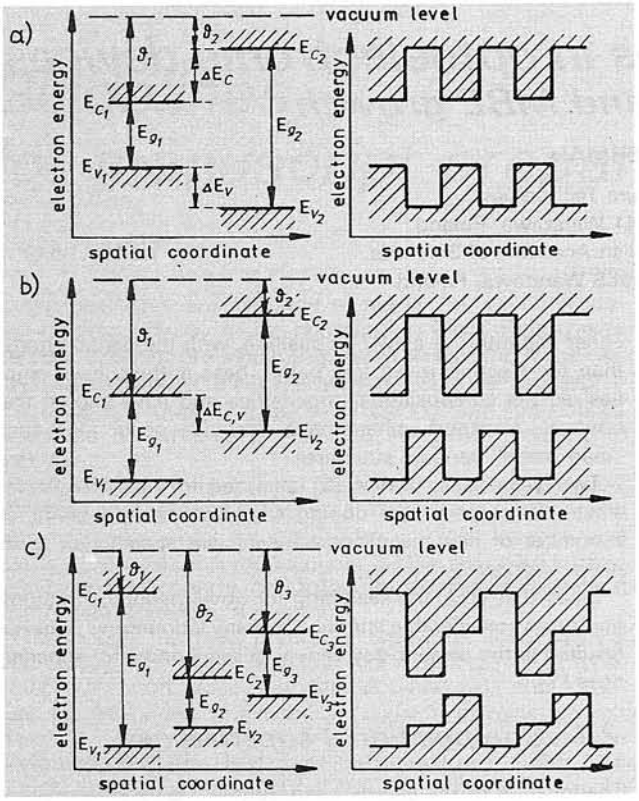

Fig. 1. Localization of the conduction and valence band-edges in relation to the vacuum level (left side) for the constituent compounds (not in touch) and for different types of compositional superattices (right side): a) type I superlattice, b) type II superlattice, c) polytype superlattice (from Ref. [1])

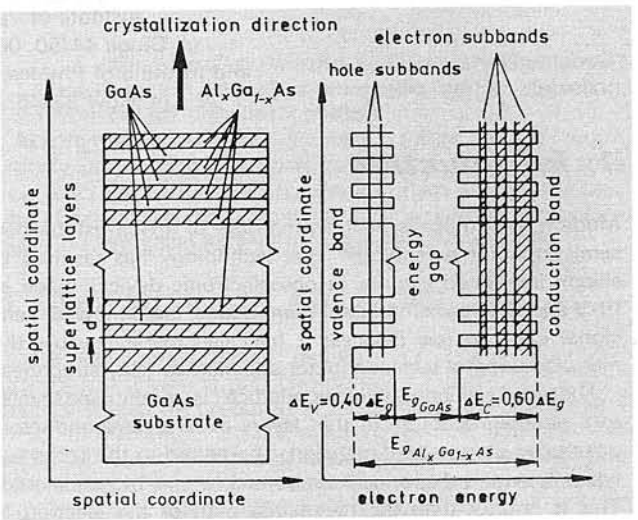

Fig. 2. Schematic illustration of layer sequence (left side), and of real-space energy band profile (right side) of the $GaAs-Al_xGa_{1-x}As$ superlattice (from Ref. [1])

Another class of type I superlattices form the so called strained-layer superlattices (SLS) [5]. These are high-quality superlattices grown from lattice-mismatched materials. The layers in these structures are kept sufficiently thin to ensure that the lattice mismatch is totally accommodated by layer strains, therefore the misfit deffects are not generated.

Five materials are usually chosen for growing SLSs. These are: $GaAs-In_xGa_{1-x}As$, $GaAs-GaAs_xP_{1-x}$, $GaP-GaAs_xP_{1-x}$, ZnS–ZnSe and GaSb–AlSb. It should be noticed, however, that SLS structures can be grown from a wide variety of lattice-mismatched materials.

Among type I superlattices also the semimetallic-semiconductor structures have interesting features. A typical representative of such superlattice is HgTe–CdTe superlattice [6]. Typically it consists of distinct, 18 nm thick layers of HgTe (a negative-gap semi-metallic compound) and 4 nm thick layers of CdTe (a wide-gap semiconductor with an energy gap of 1.49 eV at 300 K) in alternation. The whole energy gap difference ΔE_g, which is equal to the energy gap of CdTe is thus located solely in the conduction band in this superlattice. This leads to the rather unique relation for the conduction band discontinuity $\Delta E_c = \Delta E_g = E_g(\mathrm{CdTe})$.

The family of type I superlattices is completed by the silicon based ones. Within the confines of silicon materials technology the number of feasible superlattice structures is greatly limited.

With regard to conventional layered structures, the $Si-Si_{1-x}Ge_x$ system is the prototype for silicon superlattices [5]. Beyond the $Si-Si_{1-x}Ge_x$ crystalline system the silicon technology offers some novel possibilities.

The first is an amorphous superlattice made of hydrogenated amorphous silicon (a–Si:H) and hydrogenated amorphous germanium (a–Ge:H) (or silicon nitride $a-SiN_x$:H, or silicon carbide $a-Si_{1-x}C_x$:H) that are neither lattice-matched nor epitaxial, yet with interfaces that are essentially defect-free and nearly atomically sharp [1]. The second is an MOS (metal-oxide-silicon) configuration with a grided metal electrode made up of fine parallel metal lines uniformly spaced on the oxide layer.

In the type II compositional superlattices the conduction band of one material is close to the valence band of the other. This causes a spatial separation of carriers confined in the quantum wells. Electrons are confined in quantum wells existing in the first semiconductor, while holes are localized in the wells within the second semiconductor. Thus, we are dealing in these multilayer structures with an "indirect band gap in the real space" (this can be compared with the "indirect band gap in momentum space" met in many bulk semiconductors).

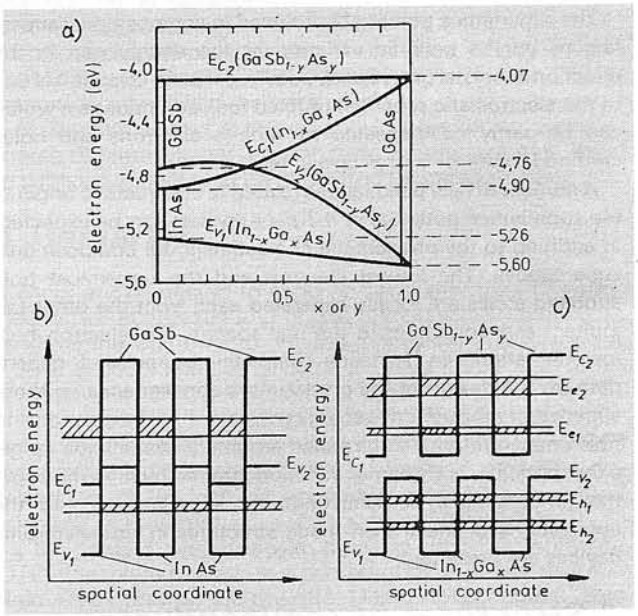

Fig. 3. Band-edge energies with respect to the vacuum level versus alloy composition in $In_{1-x}Ga_xAs$ and $GaSb_{1-y}As_y$ (a), and schematics of the energy diagrams of two superlattice systems, the InAs–GaSb (b), and $In_{1-x}Ga_xAs-GaSb_{1-y}As_y$ (c) superlattices. Shaded areas show the subbands and spatial regions where the carriers are confined (from Ref. [7])

The first system which has been proven to create type II superlattices is based on the ternaries $In_{1-x}Ga_xAs$ and $GaSb_{1-y}As_y$, with the limiting case of the InAs—GaSb superlattice for $x=0$ and $y=0$ [7].

According to the available data on the electron affinity and the energy gap for the two binary materials, the conduction band-edge in InAs is at 0.14 eV below the valence band-edge in GaSb. For the two ternaries the energy gap partly overlap, with the limiting case of a complete overlap for $x=1$ and $y=1$ (this is the GaAs energy gap).

If the ternaries $In_{1-x}Ga_xAs$ and $GaSb_{1-y}As_y$ are selected in such a way that $y=0.918\,x+0.082$, then a perfect lattice match is obtained at the hetero-interfaces of the superlattice. The band-edge energies versus compound compositions as well as the schematic energy diagrams for the type II superlattices made of this materials are shown in Fig. 3.

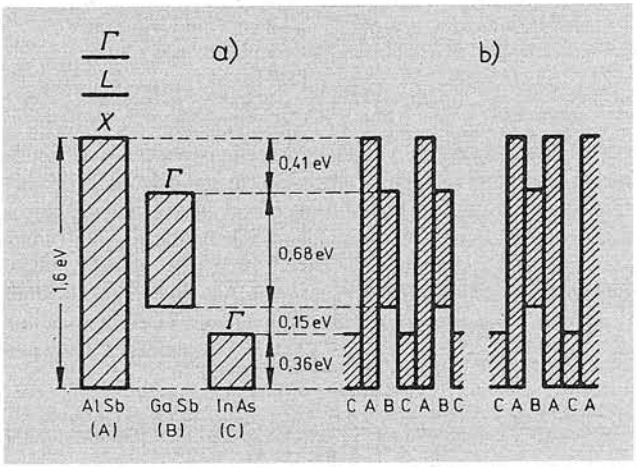

Fig. 4. a) Estimated band-edge energies of AlSb relative to those of GaSb and InAs (the hatched areas indicate the energy gaps); b) energy diagrams of two kinds of polytype superlattices (from Ref. [1])

The third type of compositional superlattices constitute the polytype superlattices. As discussed earlier, polytype superlattices can be obtained by addition of AlSb to the InAs—GaSb material system (see Fig. 1c). The band-edge energies of AlSb relative to those of GaSb and InAs are illustrated in Fig. 4a. The basic elements involved in polytype superlattices are: BAC, ABCA, ACBCA,... multi-heterojunctions (Fig. 4b) with A standing for AlSb, B for GaSb and C for InAs.

2.2. Doping superlattices

The unusual electronic properties of doping superlattices derive from the specific nature of the superlattice potential which, in this case, is the space charge potential of ionized impurities in the doping layers [3]. This is in contrast to the compositional superlattices, in which the superlattice potential originates from the different band gap values of their constituent materials. The space charge potential in the doping superlattices modulates the band-edges of the host material in such a way that electrons and holes become spatially separated. This separation can be made nearly perfect by the appropriate choice of the design parameters, which are the doping concentrations and the layer thicknesses.

One of the attractive features of doping superlattices is that any semiconductor that can be doped both n- and p-type in a well controlled way can be used as the host material. GaAs grown by MBE is used most frequently, but also Si, and PbTe or $Pb_{1-x}Sn_xTe$ compounds have been proposed as well [1].

Let us assume a semiconductor with a band gap E_g, and a static dielectric constant ε, which is modulated by periodic n- and p-doping in the z-direction. Although the doping profiles $N_D(z)$ and $N_A(z)$ may have any arbitrary shape, for the sake of simplicity only the simplest case of constant and equal doping concentrations $N_A=N_D$ within the n- and p-doped regions of thicknesses $d_n=d_p=d/2$ will be considered here. Also the possibility of impurity band formation and the posssible random inhomogeneities in the distribution of the impurity atoms are neglected here.

In such macroscopically compensated structure all impurities will be ionized in the ground state due to recombination of the electrons from donors with the holes from acceptors. Therefore, a periodic parabolical space-charge (or built-in) potential $V_D(z)$ exists in the crystal due to the donors (positively charged) and the acceptors (negatively charged). This potential is superimposed to the crystal lattice potential, and modulates the conduction and valence band-edges as shown schematically in Fig. 5.

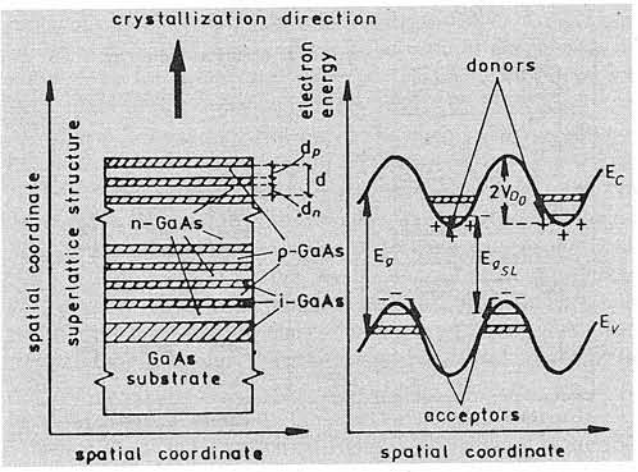

Fig. 5. Layer sequence (left side) and real-space energy band profile (right side) of the GaAs doping superlattice (n-i-p-i—crystal) (from Ref. [1])

The motion of charge carriers in the z-direction is then quantized by the superlattice potential $V_D(z)$. The effective band gap $E_{g,SL}$ of the superlattice, i.e. the distance between the bottom of the lowest conduction subband at the energy $E_{c,o}$ above the conduction band minimum and the top of the uppermost valence subband at $E_{v,o}$ below the valence band maximum becomes

$$E_{g,SL} = E_g - 2V_D + E_{c,o} + |E_{v,o}| \qquad (1)$$

It is obvious that the effective band gap $E_{g,SL}$ is strongly reduced below the value E_g of the unmodulated host material, and that it depends on V_D, i.e. on doping concentrations and the layer thicknesses.

2.3. Doped compositional superlattices

In standard compositional superlattices the layers of the constituent semiconductors are undoped. Therefore, the quantum wells can be treated as square-shaped (see Fig. 2). The situation will be changed if one of the semiconductors of the superlattice, e.g. the wide-gap semiconductor will be doped with donors.

This special situation has been demonstrated in the GaAs—$Al_xGa_{1-x}As$ modulation doped superlattice [8]. Since the GaAs conduction band-edges lie lower in energy than the $Al_xGa_{1-x}As$ donor states do, electrons released from the donors into the $Al_xGa_{1-x}As$ crystal lattice can diffuse toward the undoped GaAs regions gaining thus spatial separation from their parent ionized donors. Finally, all mobile carriers become confined in the GaAs layers where they can move in the

directions parallel to the hetero-interface without being scattered by ionized impurities. This leads to considerable enhancement of the mobility of these electrons in the narrow-gap semiconductor layers.

The spatial transfer of mobile charge carriers create, however, also space charge regions of alternating sign in the superlattice, what results in a periodic bending of the band-edges, as shown in Fig. 6. The effect of mobility enhancement is most pronounced in these superlattices at low temperatures where the phonon scattering processes competing with the Coulomb scattering processes (largely diminished) are weak. Peak mobilities in excess of 10^6 cm^2/(V · s), at 4.2 K have been achieved.

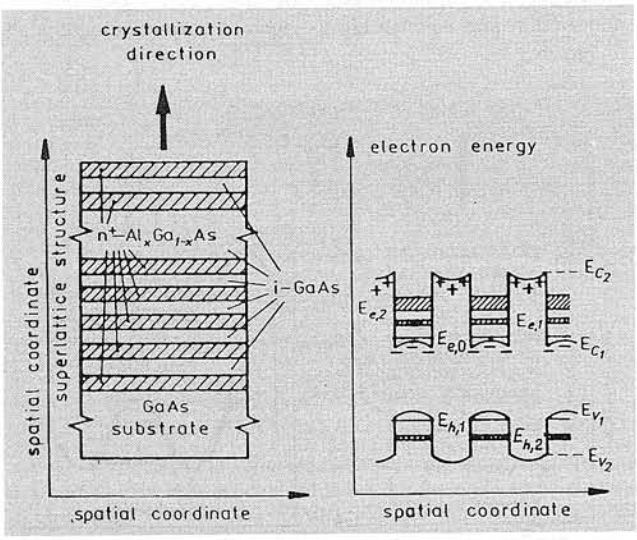

Fig. 6. Layer sequence (left side) and real-space energy band diagram (right side) of the modulation doped superlattice (from Ref. [1])

situ by surface analytical techniques, like reflection high energy electron diffraction (RHEED).

The experimental geometry of RHEED is illustrated in Fig. 8. Electrons having energy of typically 5 ÷ 20 keV are incident on the substrate at a variable glancing angle ($0 \leqslant \theta \leqslant 5°$). The diffraction of the incoming primary beam leads to the appearance of intensity-modulated streaks (or rods) perpendicular to the shadow edge superposed on a fairly uniform background which is due to inelastically scattered electrons. It is obvious from the figure why this geometry is ideal for combination with MBE, where it is desirable to have the molecular beams impinging on the substrate surface at near-normal incidence.

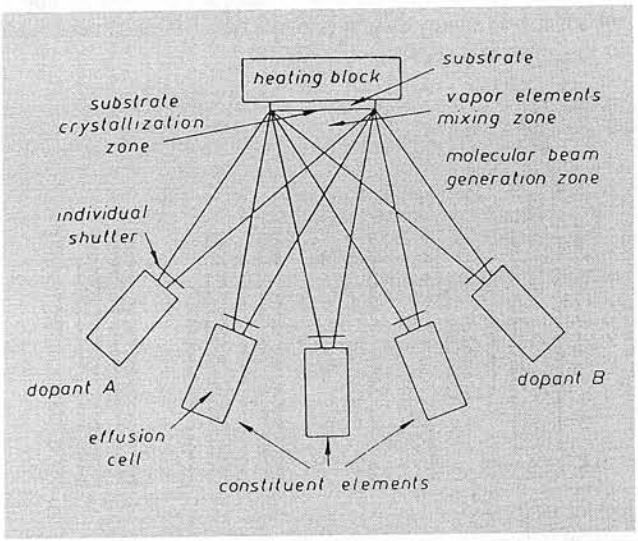

Fig. 7. Schematic illustration of the essential parts of a MBE growth system. Three zones where the basic processes of MBE take place are indicated (from Ref. [1])

3. Crystallization of superlattice structures by molecular beam epitaxy

A variety of different growth techniques has been used to grow superlattice structures, but so far only few of them seem to be well adapted for satisfying the stringent requirements of such multilayer structures [1].

Molecular beam epitaxy (MBE) in its essential form combined with various innovative concepts of crystallization under ultra-high vacuum [9] offers greatest hope of achieving nearly perfect structures, desired for research and for device applications.

In MBE, thin films crystallize via chemical reactions between thermal energy molecular or atomic beams of the constituent elements (or gaseous reactants containing the constituent elements) and a substrate surface which is maintained at an elevated temperature in ultra-high vacuum (UHV). The growth rate of typically 1 μm/h (1 monolayer/s) is low enough to ensure the surface migration of the impinging species on the growing surface. Consequently, the surface of the grown film is very smooth (on the macroscopic scale). Simple mechanical shutters in front of the beam sources are used to interrupt the beam fluxes, i.e. to start and to stop the deposition and/or doping. Changes in composition and doping can thus be abrupt on an atomic scale. The essential elements of a MBE system are shown schematically in Fig. 7 [9].

One has to notice, that a great advantage of the MBE growth technique is the possibility of controlling the growth process *in*

In 1983 damped oscillations in the intensity of the specular and the diffracted beams of the RHEED pattern during MBE growth were observed for the first time.

A typical example of the specular beam intensity oscillations obtained during MBE growth of GaAs on the GaAs(001) substrate surface is shown in Fig. 9. The period of oscillation corresponds exactly to the growth of a single monolayer, i.e. a complete layer of Ga and As atoms ($a_o/2$ in the [001]

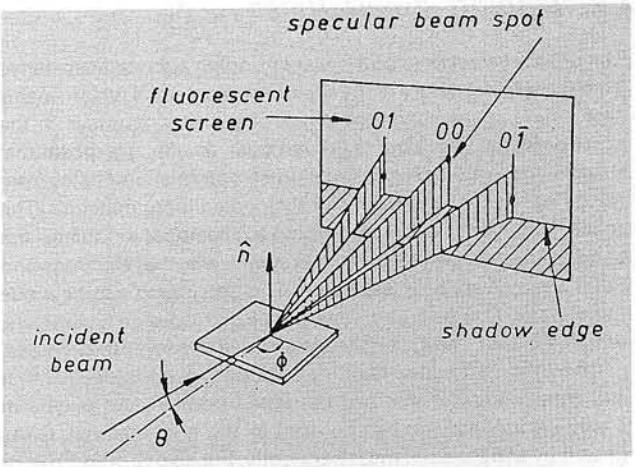

Fig. 8. Schematic diagram of RHEED geometry showing the incident beam at an angle 0 to the surface plane; azimuthal angle φ. The elongated spots indicate the intersection of the Ewald sphere with the 01, 00 and 01 rods (from Ref. [9])

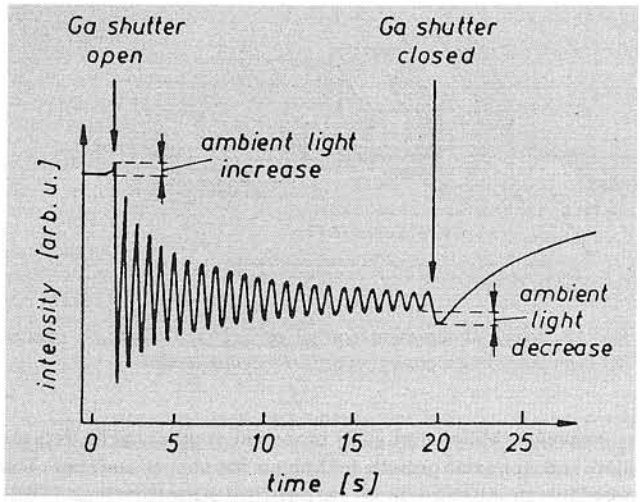

Fig. 9. Intensity oscillations of the specular beam in the RHEED pattern from GaAs(001) surface at [110] azimuth (from Ref. [9])

direction). A growth interruption was made after nearly 20 s of the MBE growth, i.e. the Ga source shutter was then closed while leaving the As source shutter open. During the growth interruption period, the specular beam intensity increased again. This process is attributed to the recovery of the surface smoothness, which in turn is caused by the surface migration or the sublimation of atoms adsorbed to the crystalline surface of the grown epilayers.

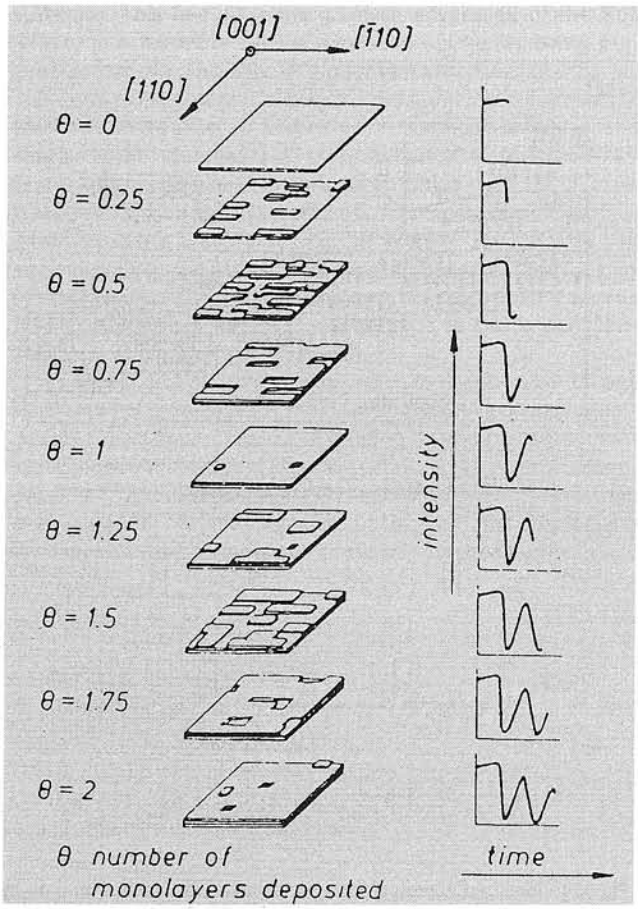

Fig. 10. Real space representation of the formation of the first two complete monolayers of GaAs(001) in relation to RHEED intensity oscillations, according to the first-order growth model. Here θ is the fractional layer coverage (from Ref. [9]).

In Fig. 10 a real space representation of the formation of the first two complete layers of GaAs is shown. This illustrates how the oscillations in the intensity of the specular beam occur. There is a maximum reflectivity for the initial and final smooth surfaces and a minimum for the intermediate stage when the growing layer is approximately half complete.

In MBE of superlattices, epitaxy should occur principally by a two-dimensional layer-by-layer process. In order to get this mode of MBE Sakamoto et al. [10] developed a special MBE growth technique named phase-locked epitaxy (PLE). It is based on the following idea. Long continuing intensity oscillations of the RHEED pattern in the [100] azimuth on a (001) oriented substrate are recorded during MBE growth of GaAs and $Al_xGa_{1-x}As$. Using these oscillations, growth rates of the growing compounds and the Al mole fraction x of the ternary compound are accurately monitored during the growth. The phase of the RHEED oscillations is analyzed by computer and molecular beam source shutters are operated at a particular phase of the oscillations initiating the growth after a definite interruption for getting the maximum of the RHEED intensity (maximum of the surface smoothness).

PLE was first used to grow precisely defined $(GaAs)_2(AlAs)_2$ bilayer superlattices [10]. From TEM observation of a GaAs—AlAs multilayered structure, it was verified that, one cycle of oscillations corresponds to one monolayer growth of GaAs and AlAs. The PLE has a great advantage over the conventional MBE growth method for the precise control of the growth of very thin films and superlattices because it is invulnerable to fluctuations of molecular beam flux intensity. The $(GaAs)_2(AlAs)_2$ bilayer superlattice with 699 periods, i.e. with 2796 monolayers, was grown with excellent structural quality by using the PLE method.

Neave et al. [11] examined RHEED oscillations occurring during growth of GaAs on vicinally cut (stepped) GaAs substrates at increasing growth temperatures. The principal feature of this work (Fig. 11a) is the progressive reduction in the intensity of the RHEED oscillations until a critical temperature there are no oscillations. This effect may be interpreted as a transition from low-temperature growth by two-dimensional nucleation on the terraces to a high-temperature mode where

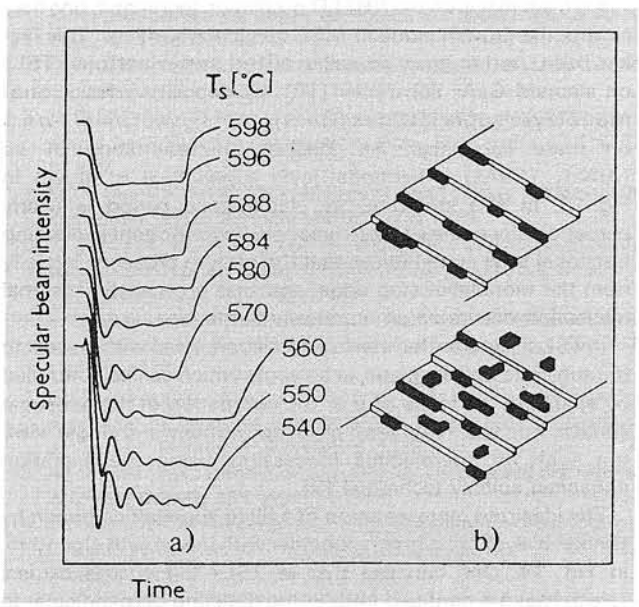

Fig. 11. a) RHEED measurements showing eventual disappearance of intensity oscillations with increasing substrate temperature T_s; b) Schematic illustration of the transition from growth by 2D nucleation to step flow (from Ref. [11])

increased mobility leads to direct incorporation of migrating adatoms into the growth front at the terrace edges. Thus, in the high-temperature regime, growth proceeds by step propagation (step-flow mode), for which the mean surface step density remains approximately constant, in contrast to the two-dimensional nucleation growth mode, in which the step density varies as on a flat surface (Fig. 11b).

Schematic illustration of the change in RHEED information as the growth mode changes from "step flow" to "two-dimensional nucleation" is shown in Fig. 12.

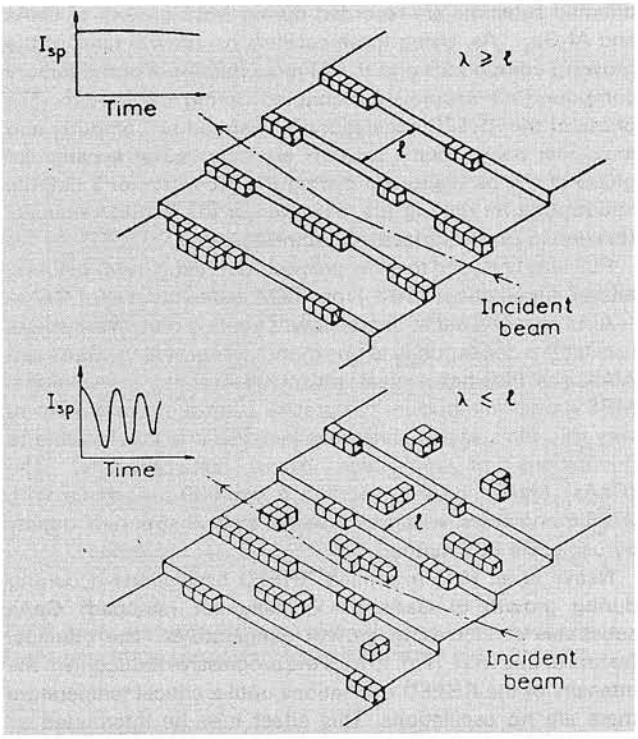

Fig. 12. Schematic illustration of the method of determining the surface diffusion parameters (from Ref. [11])

It is clear that with the RHEED oscillation technique, one may control the growth mode in MBE on vicinal surfaces. This fact has been used to grow so-called **tilted superlattices** (TSL) on stepped GaAs substrates [12], by depositing **fractional monolayer superlattices** $(GaAs)_m(AlAs)_n$ with $p=m+n\approx 1$ on these substrates. An idealized representation of an $(AlAs)_{1/2}(GaAs)_{1/2}$ fractional layer superlattice is shown in Fig. 13. In this structure, the superlattice period is nearly perpendicular to the growth direction. It is important in creating fractional layer superlattices that the growth proceeds laterally from the monolayer step edge, and that no two-dimensional nucleation occurs on an atomically flat terrace.

In TSL structures the interface planes are tilted with respect to the substrate surface plane, at an angle which can be controlled by adjusting the value of p or the orientation of the substrate surface. The first TSLs were produced entirely in a single MBE run, with no intermediate processing, using the migration enhanced epitaxy technique [9].

The idealized representation of a tilted superlattice grown by Gaines et al. [12] is shown, together with the growth algorithm, in Fig. 14. One can see that in TSLs the charge carriers (electrons) are confined both in the direction perpendicular to the substrate plane and parallel to it, approximating quantum wires [4]. Until present TSLs have not successfully been used to form two-dimensional confinement structures with good electrical and optical properties.

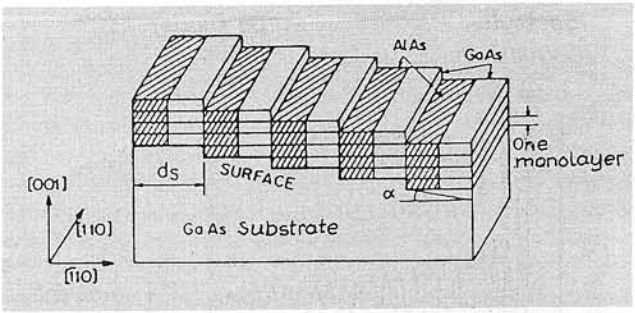

Fig. 13. Idealized representation of an $(AlAs)_{1/2}(GaAs)_{1/2}$ fractional-layer superlattice grown on a (001) vicinal surface.

However, Miller et al. [13] proposed another cyclic deposition and epitaxial growth technique for vicinal surfaces. The resulting structures, named **serpentine superlattices** (SSL) for their purposefully meandering shapes, may be employed to obtain by MBE quantum wires (QWR) [4]. SSL are produced with a cyclic deposition and growth technique on vicinal substrates, taking the relative coverage between successive deposition cycles as a variable, well controlled parameter. During such a growth with MBE, the shuttering of the molecular beams is under computer control and may be changed each cycle by a certain amount relative to the other cycles.

Smoothly sweeping the per-cycle coverage back and forth through a range including monolayer coverage gives a structure with a continuously varying tilt, as is schematically represented in Fig. 15. Two-dimensional electronic confinement may be obtained at the wide places in the winding wells, where the

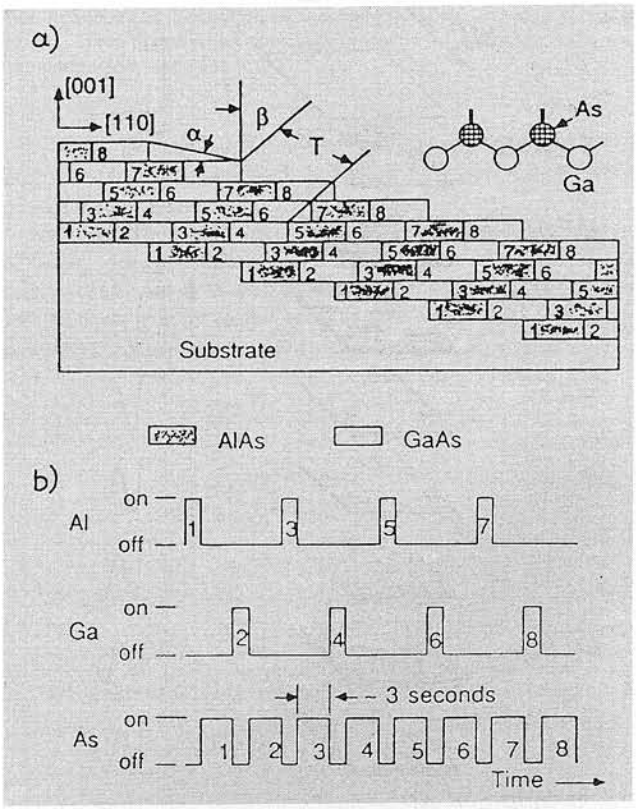

Fig. 14. Idealized representation of a tilted superlattice grown by migration enhanced epitaxy: a) Cross section, perpendicular to the step edges, of a superlattice with $p=1.25$. The inset shows the arrangement of the As bonds with respect to the step edges; b) Detail of growth, showing the order of atomic depositions. Numbers in a) refer to partial monolayers deposited in b) (from Ref. [12])

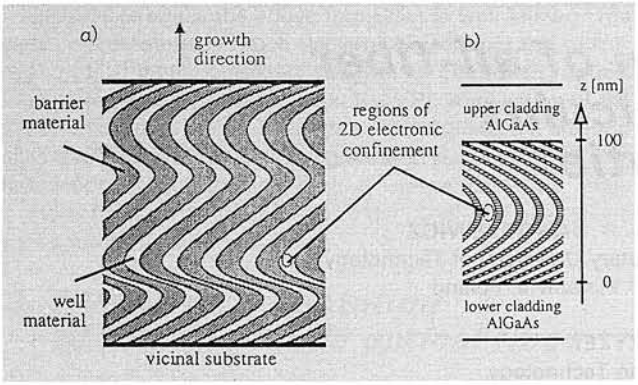

Fig. 15. A serpentine superlattice cross section is shown: (a) that would result from sweeping the per-cycle coverage back and forth through a range that includes exact monolayer coverage. At such places, where the tangent to the structure is vertical, electronic states are confined to two dimensions. The 2D potential energy minima near these regions may be characterized by the lateral barrier and well widths, lateral barrier height and the local curvature of the SSL; (b) most of the simulated and grown structures have been single-crescent., parabolic geometries with barriers cladding the SSL region above and below (from Ref. [13])

structure turns a corner. The shape near these regions determines the energy spectrum of the confinement. It is important to notice that the confinement in the SSLs is insensitive to errors in the absolute growth rates. An error shifts the vertices of the parabolas up or down in the growth direction but does not change their shape. Thus a confinement may be obtained that is quite insensitive to growth rate variations across the entire substrate. This feature is the greatest. advantage of the SSL structure. A particular device application currently being pursued is that of using SSL in a quantum wire laser [13].

Among doping superlattices, the most interesting one is the **saw-tooth doping superlattice**. It has been proposed and experimentaly demonstrated by Schubert et al. in 1985 [14]. The doping profile in this GaAs superlattice consists of Dirac delta-functions, as shown in Fig. 16. This profile is generated by interrupting the usual "crystal growth mode" during MBE [9], and continuing growth by the "impurity growth mode", i.e. by closing the Ga-source and opening the respective Be- and Si-dopant sources, while the As source is kept open continuously at all time of the growth.

The donor and acceptor atoms are thus localized within one single atomic monolayer of the zincblende lattice. Consequently, the superlattice consists of doping spikes of two-dimensional concentration $N_D(2D) = N_A(2D) = 5 \cdot 10^{12}$ cm^{-2}, separated by 10 nm thick undoped GaAs layers. Electrons from their parent donors recombine with holes from acceptors, and consequently the superlattice is depleted of free carriers.

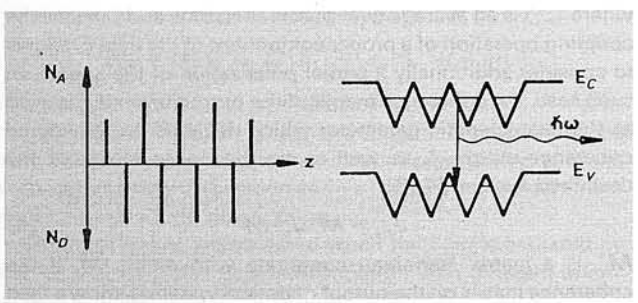

Fig. 16. GaAs saw-tooth superlattice: doping profile of the superlattice, consisting of Dirac-delta functions (spike-doping, left side), and conduction and valence band potential in the direction of crystal growth (right side); from Ref. [14]

However, the donor and acceptor charge distribution of the superlattice causes a saw-tooth-shaped conduction and valence band potential, as illustrated in Fig. 16. Nonequilibrium electrons and holes generated occasionally, by optical excitation, or by electrical injection in the superlattice structure occupy quantized energy levels in the V-shaped potential wells, owing to the quantum size effect. These excess electrons and holes recombine in a "quasi-vertical" mode (see Fig. 16), owing to the spatial proximity of quantized electron and hole states.

This results in a short carrier lifetime and high radiative efficiency. This property has enabled the construction of a saw-tooth superlattice light. emitting diode [14], which is extremely stable in the peak wavelength even at the changes of the excitation (injection) current over four orders of magnitude (from 0,2 mA to 2 A).

Concluding the considerations concerning the MBE growth of superlattice structures it should be emphasised that MBE can be used to achieve extreme dimensional control in both chemical composition and doping profiles. Single crystal superlattice structures with layer thickness of only few atomic layers can be easily grown with many semiconductor materials. The extraordinary versatility of this growth technique, coupled with the recent appearance of multichamber, multifunction MBE systems [9] makes it one of the most important device fabrication technique.

References

1. *M. A. Herman:* Semiconductor superlattices. Akademie Verlag, Berlin 1986 (Russian translation by Mir, Moscow 1989).
2. *L. Esaki* and *R. Tsu:* Superlattice and negative differential conductivity in semiconductors. IBM J. Res. Dev., **14** (1970) p. 61.
3. *G. H. Döhler:* Electron states in crystals with *n-i-p-i* superstructure. Phys. Status Solidi B, **52** (1972) p. 79, and p. 533.
4. *G. Weisbuch* and *B. Vinter:* Quantum semiconductor structures fundamentals and applications. Academic Press, Boston 1991.
5. *T. P. Pearsall* (ed.): Strained-Layer Superlattices: Materials Science and Technology; vol. 33, and *R. K. Willardson* and *A. C. Beer* (eds.) in: Semiconductors and Semimetals, Academic Press, Boston 1991.
6. *M. A. Herman and M. Pessa:* $Hg_{1-x}Cd_xTe - Hg_{1-y}Cd_yTe$ ($0<x, y<1$) heterostructures: properties, epitaxy and applications. J. Appl. Phys., **57** (1985) p. 2671.
7. *L. L. Chang* and *L. Esaki:* Electronic properties of InAs–GaSb superlattices. Surface Sci., **98** (1980) p. 70.
8. *H. R. Dingle* et al: Electron mobilities in modulation-doped semiconductor heterojunction superlattices, Appl. Phys. Lett., **33** (1978) p. 665.
9. *M. A. Herman* and *H. Sitter:* Molecular beam epitaxy fundamentals and current status. Springer Verlag, Berlin 1989.
10. *T. Sakamoto* et al.: Well defined superlattice structures made by phase-locked epitaxy using RHEED intensity oscillations. Superlattices Microstruct., **1** (1985) p. 347.
11. *J. H. Neave* et al.: RHEED oscillations from vicinal surfaces - a new approach to surface diffusion measurements. Appl. Phys. Lett., **47** (1985) p. 100.
12. *J. M. Gaines* et al.: MBE growth of tilted GaAs/AlAs superlattices by deposition of fractional monolayers on vicinal (001) substrates. J. Vac. Sci. Technol. B, **6** (1988) p. 1378.
13. *M. S. Miller* et al.: Serpentine superlattices: concept and first results. J. Crystal Growth, **111** (1991) p. 323.
14. *E. F. Schubert, A. Fischer* and *K. Ploog:* GaAs saw-tooth superlattice LED operating monochromatically at $\lambda \geqslant 0.9$ μm. Electron. Lett., **21** (1985) p. 411.